Anomalous pinning behavior in an incommensurate two-chain model of friction

Takaaki Kawaguchi
Department of Technology, Faculty of Education, Shimane University, 1060 Nishikawatsu, Matsue 690-8504, Japan

Hiroshi Matsukawa
Department of Physics, Osaka University, 1-16 Machikaneyama Toyonaka, Osaka 560-0043, Japan

(Received 15 May 1998)

Pinning phenomena in an incommensurate two-chain model of friction are studied numerically. The pinning effect due to the breaking of analyticity exists in the present model. The pinning behavior is, however, quite different from that for the breaking of the analyticity state of the Frenkel-Kontorova model. When the elasticity of chains or the strength of interchain interaction is changed, pinning force and maximum static frictional force show anomalously complicated behavior accompanied by a successive phase transition and they vanish completely under certain conditions. [S0163-1829(98)03947-2]

I. INTRODUCTION

In recent years, the study of friction has been attracting much attention in physics.[1] Nanoscale frictional phenomena have been examined experimentally using frictional force microscopes,[2] quartz microvalance techniques,[3] and so on. In theoretical studies, the Frenkel-Kontorova (FK) model[4] and its related ones have been employed as a promising model of such nanoscale friction by several researchers.[5–8] The FK model, in general, consists of an atomic chain on a substrate with periodic potential. In the chain harmonic force works between neighboring atoms. When the mean atomic distance and the period of the potential is incommensurate, the FK model shows a phase transition, which has been discussed in detail by Aubry and co-worker.[9,10] Hence this phase transition is called the Aubry transition. The Aubry transition has the following features. When the amplitude of the substrate potential is smaller than a certain critical value, the lowest phonon excitation is gapless and, therefore, a free-sliding mode appears. This means vanishing maximum-static frictional force. Above the critical amplitude, however, the atoms in the chain are pinned strongly nearby the potential minima and a finite gap exists in the phonon excitation. This state is called the breaking of the analyticity state. Then finite energy is needed to slide the chain, and, therefore, the maximum-static frictional force becomes finite. The extended FK model, which consists of interacting two deformable chains, also have been investigated so far. The static structural properties of two-chain models have been investigated in Refs. 11–14, where each chain is often treated as a continuum elastic line. The continuum approximation works effectively in the study on the commensurate-incommensurate transition.[12] However, the pinning effect that arises from the discrete nature of lattices are smeared out inevitably. In other words, the Aubry transition never occurs in the continuum models. On the basis of a two-chain model with discrete lattice structures, Matsukawa and Fukuyama investigated the static and the kinetic frictional forces.[15,16] The model proposed in their study consists of two atomic chains, where interchain atomic force works between atoms in one chain and in another and harmonic force works between neighbor atoms in each chain. In some cases of elastic parameters of chains, they found that the maximum static frictional force for the two-chain model becomes larger than that for the FK model with the same strength of the interchain interaction. Furthermore, they discussed the relationship between the strength of the maximum-static frictional force and the velocity dependence of kinetic frictional force.

In this paper, we revisit the two-chain model of friction employed in Ref. 15 and examine the frictional phenomena in a wide range of model parameters. In particular, pinned states are investigated thoroughly in connection with the breaking of the analyticity state due to the Aubry transition. It turns out that the maximum-static frictional force shows complicated behavior against the change in elastic parameters and vanishes completely in certain conditions. This anomalous pinning behavior is discussed in relation to the static lattice structures. We also focus on the velocity dependence of the kinetic frictional force in sliding states.

II. TWO-CHAIN MODEL OF FRICTION

The two-chain model of friction employed here is summarized in the following.[15] We consider two atomic chains, i.e., an upper chain and a lower chain. Each atom has a one-dimensional degree of freedom parallel to the chain. Intrachain interaction with harmonic form and interchain interaction are taken into consideration. The effects of energy dissipation are assumed to be proportional to the difference between the velocity of each atom and that of the center of gravity of the chain. The upper chain is driven by the external force parallel to the chain. Assuming overdamped motion, we get the equations of motion of the atoms in the upper and the lower chains given by

$$m_a\gamma_a(\dot{u}_i-\langle\dot{u}_i\rangle_i)=K_a(u_{i+1}+u_{i-1}-2u_i)+\sum_{j\in b}^{N_b}F_I(u_i-v_j)+F_{ex}, \quad (1)$$

$$m_b\gamma_b(\dot{v}_i-\langle\dot{v}_i\rangle_i)=K_b(v_{i+1}+v_{i-1}-2v_i)+\sum_{j\in a}^{N_a}F_I(v_i-u_j)-K_s(v_i-ic_b), \quad (2)$$

where u_i (v_i), m_a (m_b), γ_a (γ_b), K_a (K_b), and N_a (N_b) are the position of the ith atom, the atomic mass, the parameter of energy dissipation, the strength of the interatomic force, and the number of atoms in the upper (lower) chain, respectively. K_s denotes the strength of the interatomic force between the lower chain and the substrate, which is necessary to bind the lower chain. $\langle\ \rangle_i$ represents the average with respect to i. F_I and F_{ex} are the interchain force between the two atomic chains and the external force, respectively. The interchain atomic potential is chosen as follows:

$$U_I = -\frac{K_I}{2}\exp\left[-4\left(\frac{x}{c_b}\right)^2\right], \tag{3}$$

where K_I is the strength of the interchain potential, and c_b the mean atomic spacing of the lower chain. The interatomic force is given by $F_I(x) = -(d/dx)\,U_I$. The time-averaged total frictional force of the present model is given by

$$F^{\mathrm{fric}} = -\sum_{i\in a}^{N_a}\sum_{j\in b}^{N_b}\langle F_I(v_i - u_j)\rangle_t = N_a\langle F_{ex}\rangle_t. \tag{4}$$

This expression of the frictional force is valid for both static and kinetic ones. The form of interchain force, $F_I(x) = -(d/dx)\,U_I$, is approximated in the following two limiting cases.[17] When the atoms in the lower chain are rigid and fixed at the regular sites, which corresponds to the case of $K_b/K_a \to \infty$ or $K_s/K_a \to \infty$, the interchain force that acts on the upper chain is approximated by one term in a Fourier series:

$$\sum_{j\in b}^{N_b} F_I(u_i - v_j)\Big|_{v_j = jc_b} \simeq -0.47K_I\sin\left(2\pi\frac{u_i}{c_b}\right). \tag{5}$$

Then the two-chain model is reduced to the FK model. In the opposite limit, when the upper chain is fixed at the regular sites ($K_a/K_b \gg 1$), the interchain interaction that acts on the lower chain is also described by one term in a Fourier series:

$$\sum_{i\in a}^{N_a} F_I(u_i - v_j)\Big|_{u_i = ic_a} \simeq -0.83K_I\sin\left(2\pi\frac{v_j}{c_a}\right), \tag{6}$$

where c_a is the mean atomic spacing of the upper chain. These approximations on the interchain force are valid only in the above two limiting cases on elastic parameters, and they may break in intermediate cases. This is a crucial point in the following discussion.

III. NUMERICAL METHOD

For the numerical simulation of the model, the Runge-Kutta (RK) formula is employed to solve the equations of motion. The periodic boundary conditions are employed in both chains. Hence, the ratio c_a/c_b is equal to N_b/N_a, where N_a and N_b are the numbers of atoms in the upper and lower bodies.

$$\frac{c_a}{c_b} = \frac{N_b}{N_a} = \frac{233}{144} = 1.618\ldots, \tag{7}$$

where the ratio is determined by using a continued-fraction expansion of the golden mean to emulate incommensurability. Throughout the present study we set the values of the model parameters as

$$N_a = 144, \quad N_b = 233, \quad c_a = 1.618\ldots, \quad c_b = 1,$$
$$m_a = m_b = 1, \quad K_a = 1, \quad \gamma_a = \gamma_b = 1. \tag{8}$$

We control the elasticity of chains by changing the spring constants K_s and K_b, and the strength of interchain interaction by K_I.

In numerical simulations we mainly employ an initial atomic configuration where atoms are located at regular sites periodically. During the RK steps the chains are relaxed to stable states and finally reach there. In Sec. IV A 5 we will refer to the effect of the initial atomic configuration in connection with pinning behavior.

We employ the following numerical criterion and methods in the calculations of several quantities. If $\dot{u}_i$ and $\dot{v}_i$ calculated during the RK steps satisfy a velocity condition, $\sqrt{[\Sigma^{N_a}{}_i(\dot{u}_i)^2 + \Sigma^{N_b}{}_i(\dot{v}_i)^2]/(N_a+N_b)} < 10^{-10}$, the RK calculation is stopped, and the state obtained then is considered to be static. The phonon frequency is calculated using a dynamical matrix for this stationary state. The maximum-static frictional force is evaluated as the critical force above which the velocity condition is not satisfied. Using the criterion, the difference between pinned and sliding states is distinguishable. The frictional force is calculated according to Eq. (4) or the method used in Ref. 15. In a sliding state, after the system reaches a steady state, the temporal average is performed in calculating the kinetic frictional force over a time period much longer than a time during which the center of gravity of the system moves by the system length $N_a c_a (= N_b c_b)$.

IV. RESULTS

A. Pinned states

1. Lowest phonon frequency

In this section we investigate the pinning effect of the two-chain model in the absence of external force. To investigate the feature of pinned states, we first calculate the lowest-phonon frequency, which is a significant quantity because finite lowest phonon frequency, i.e., the phonon gap, means the presence of pinning and its square is proportional to the restoring force due to pinning effects.

For the comparison with the two-chain model, we first show the squared lowest-phonon frequency (ω_{lpf}^2) of the FK model described by Eqs. (1) and (5) with $K_I = 1$ in Fig. 1. In this case the elastic parameter is K_a only, and there exists its critical value. Below the critical K_a, ω_{lpf}^2 becomes finite, corresponding to the appearance of the breaking of the analyticity state due to the Aubry transition. Above the critical K_a, ω_{lpf}^2 vanishes. The change of ω_{lpf}^2 is continuous at the critical point. Such behavior of ω_{lpf}^2 for the FK model was reported in Ref. 10. In the present study on the two-chain model we have another elastic parameter in the lower chain. Hence, we focus on the effect of the elastic relaxation of the lower chain, and then K_s and K_b are chosen as variable elastic parameters.

In Fig. 2(a) we show ω_{lpf}^2 as a function of an elastic constant K_b in the case of strong interchain interaction $K_I = 1$

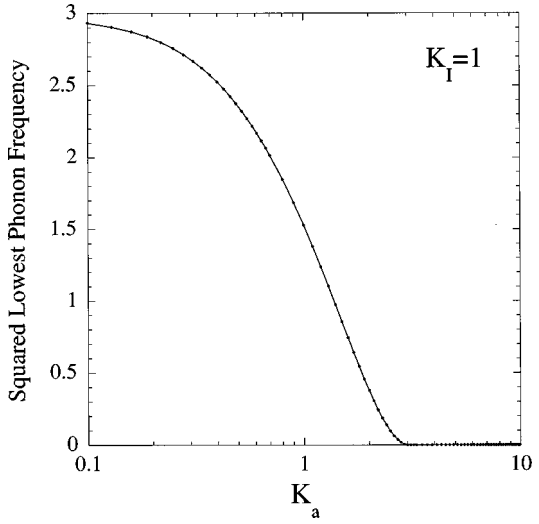

FIG. 1. Squared lowest-phonon frequency for the FK model ($K_a=K_I=1$ and $K_b=K_s=\infty$).

and $K_s=1$. The strength of the interchain interaction ($K_I=1$) is chosen to be greater than the critical value of the Aubry transition for the FK model, $K_{I,\mathrm{FK}}^{\mathrm{critical}}\approx 0.33$ for $K_a=1$. Because of strong interchain interaction, the phonon gap is finite and almost constant in the region of large value of K_b ($2.4<K_b$). However, steep valleys appear in the range $0.81<K_b<2.4$. The amount of ω_{lpf}^2 changes there more than two orders of magnitude. It is considered that ω_{lpf}^2 vanishes at each valley. The finite values of ω_{lpf}^2 at the bottom of the valleys will be due to the numerical accuracy of the present calculation and the finite magnitude of changing in K_b. When K_b becomes smaller than a certain value (≈ 0.81), ω_{lpf}^2 increases sharply and then becomes almost constant. The vanishing phonon gap at each valley seems to indicate a sort of phase transition.

When the interchain interaction K_I is somewhat weakened, but its strength is still greater than $K_{I,\mathrm{FK}}^{\mathrm{critical}}$, more drastic behavior of phonon gaps is observed. Figure 2(b) shows ω_{lpf}^2 obtained for $K_I=0.45$ and $K_s=1$. Finite phonon gaps exist both in small and large K_b regimes, and steep valleys appear in the intermediate regime $0.2<K_b<0.6$. Such behavior is quite similar to that for $K_I=1$. In a wide regime, $0.6<K_b<1.4$; however, the phonon gap vanishes completely within a numerical accuracy. This regime is quite distinct from other regimes with narrow valleys seen in Fig. 2(a) as discussed in the next subsection. The anomalous behavior of the phonon gap disappears when a large value of K_s is chosen as in Fig. 2(c), where $K_s=10$ ($K_I=1$). It is obvious that the behavior of the phonon gap depends on the elastic parameter K_s as well as K_b. In Fig. 2(a) the behavior of the phonon gap looks self-similar. If this is the case, the phonon gap reveals more complicated behavior against a smaller change in K_b in the intermediate K_b regime.

The discontinuous and complicated behavior of ω_{lpf}^2 against the change in elastic parameters for the two-chain model is obviously quite different from that for the FK model shown in Fig. 1. We confirmed that the magnitude of the phonon gap at all K_b's chosen in Figs. 2(a)–2(c) is entirely insensitive to the enlargement of the system size determined by using a continued-fraction expansion of the golden mean in Eq. (7).

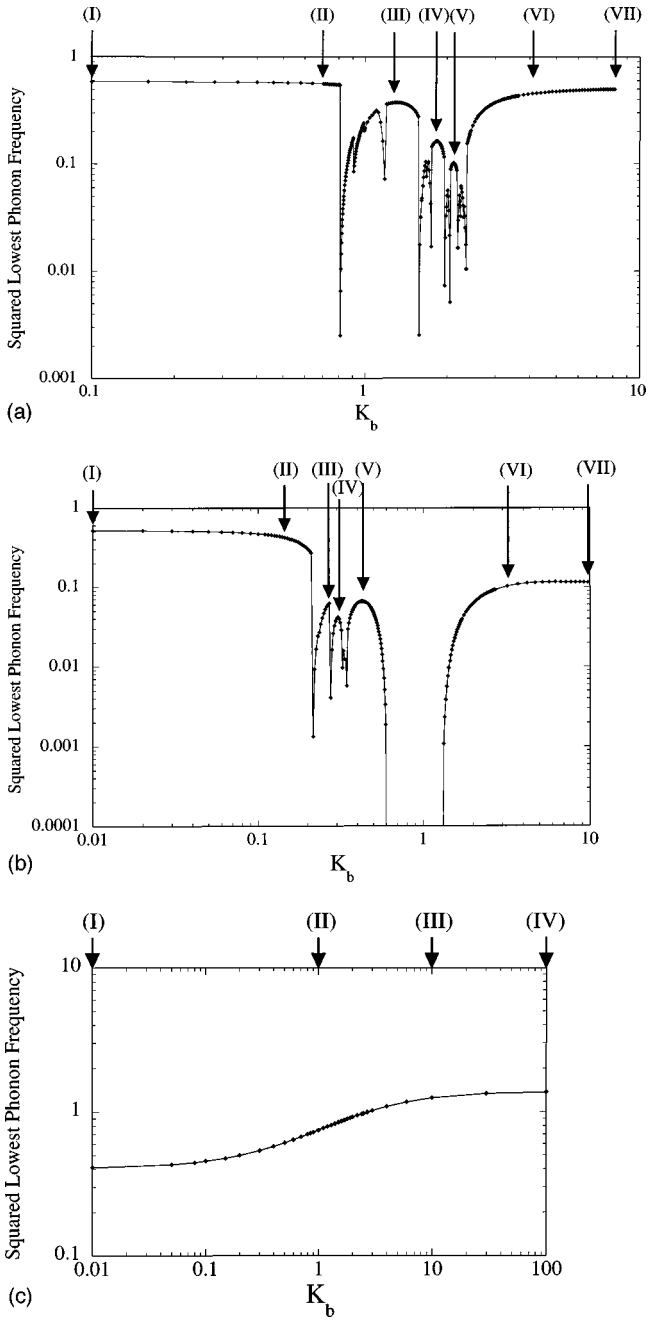

FIG. 2. Squared lowest phonon frequency vs K_b. (a) $K_I=1$ and $K_s=1$, (b) $K_I=0.45$ and $K_s=1$, and (c) $K_I=1$ and $K_s=10$. K_a is fixed at unity. We will refer to insetted numbered arrows later in Figs. 5, 6, and 8.

2. Maximum-static frictional force

Next we calculate the maximum-static frictional force numerically by applying the external force to the pinned states. Figures 3(a) and 3(b) show the maximum-static frictional force calculated for pinned states shown in Figs. 2(a) and 2(b), respectively. The maximum-static frictional force also shows anomalous behavior, which obviously reflects the phonon gap structures in Figs. 2(a) and 2(b). In Fig. 3(a), where the values of the parameters $K_I=1$ and $K_s=1$ are the

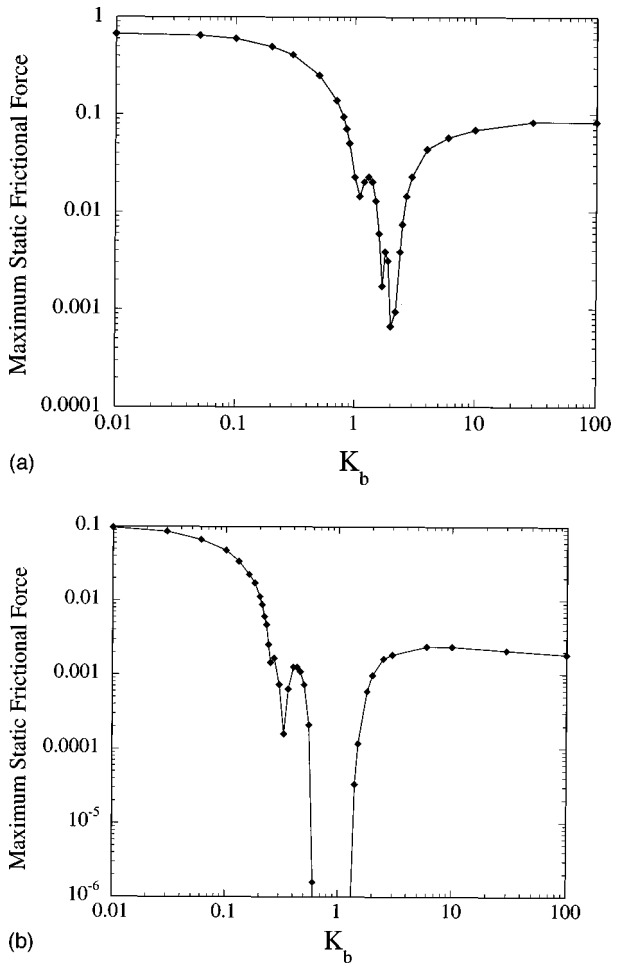

FIG. 3. Maximum static frictional force vs K_b. (a) $K_I=1$ and $K_s=1$, (b) $K_I=0.45$ and $K_s=1$. K_a is fixed at unity.

same with those in Fig. 2(a), the maximum-static frictional force shows multivalley structures. The magnitude of the maximum-static frictional force is finite in the whole K_b regime. We note that the values of K_b at the local minima and maxima of the maximum-static frictional force do not correspond exactly to those of $\omega_{\rm lpf}^2$ shown in Fig. 2(a). This may be considered to be the effect of the external force, by which the pinned lattice structures are distorted and the depinning threshold force would be affected slightly. On the other hand, as seen in Fig. 3(b) for $K_I=0.45$ and $K_s=1$, the maximum-static frictional force vanishes completely in the characteristic K_b regime where the completely vanishing phonon gap is observed in Fig. 2(b). In the case that $K_I=1$ and $K_s=10$, it is confirmed that the maximum-static frictional force as well as the phonon gap in Fig. 2(c) does not show any anomalous behavior and changes smoothly with K_b.

3. Hull functions and lattice structures

To investigate further the above anomalous pinning behavior observed for the phonon gap and the maximum-static frictional force, we analyze the lattice structures of the pinned states by examining hull functions. Although a hull function has been employed to analyze the breaking of the analyticity state for the FK model,[9,10] it has been reported that hull functions defined in two chains are also useful to analyze the lattice structures both in pinned and sliding states for the two-chain model.[17] The hull functions for the two-chain model are defined as

$$u_i = ic_a + \alpha + h_a(ic_a + \alpha), \tag{9}$$

$$v_i = ic_b + \beta + h_b(ic_b + \beta), \tag{10}$$

where h_a and h_b are the hull functions in the upper and lower chains, respectively, and α and β are constant phases. The periodicities of the hull functions are expressed as

$$h_a(x) = h_a(x + c_b), \quad h_b(x) = h_b(x + c_a). \tag{11}$$

When the chains are not deformed and hence the atoms are arrayed periodically, the interchain interaction potential is sinusoidal as mentioned in Eqs. (5) and (6), and then the position of the potential maximum in one period is located at the half of the period of the hull function $x=c_b/2$ $(c_a/2)$ for $h_a(x)$ $[h_b(x)]$ in our choice $\alpha=\beta=0$.

For the convenience of later discussions, we briefly summarize here some features of the hull function for the FK model. When the strength of the interchain interaction is less than the critical value of the Aubry transition, the hull function is smooth and continuous. Above the critical point, however, the breaking of analyticity due to the Aubry transition occurs, and then the hull function changes its form from continuous to discrete and shows a complicated structure with many gaps. Among the gaps the largest one is located at the half of the period of the hull function. The continuous form means continuous spatial atomic distribution in the underlying potential, and then no gap exists in the phonon excitation. On the other hand, the discrete one corresponds to a pinned state, which is accompanied by a finite gap in the phonon excitation. The spatial atomic distribution is vanishing at the maxima of the potential and the atoms are confined nearby the minima of the potential. Then the hull function shows the largest central gap, which characterizes the breaking of the analyticity state for the Aubry transition.

Now we consider the case of the two-chain model. Figures 4(I)–4(VII) show the hull functions h_a and h_b for several values of K_b indicated by arrows (I)–(VII) in Fig. 2(a), where the magnitudes of the parameters $K_I=1$ and $K_s=1$ are the same as those in Fig. 2(a). The hull function h_b in Fig. 4(I) $[K_b=0.1$; (I) in Fig. 2(a)] shows the largest central gap at $x=c_a/2\approx 0.809$. This gap structure is essentially the same with that for the Aubry transition in the FK model and indicates that the lower chain is in the conventional breaking of the analyticity state due to the Aubry transition. On the other hand, h_a shows a discrete feature but does not have a central gap. Such a state in the upper chain where the central gap of the hull function is absent is not well defined in the context of the conventional breaking of the analyticity state due to the Aubry transition of the FK model, but it is obviously a sort of breaking of the analyticity states because of the presence of gaps of the hull function. These gap structures of h_a and h_b remain even for $K_b=0.702$ [Fig. 4(II)]. This reflects the constant $\omega_{\rm lpf}^2$ observed in the small K_b regime $(K_b<0.81)$ in Fig. 2(a). As K_b increases further $(K_b>0.81)$, however, the central gap of h_b is destroyed and no central gap exists both in h_a and h_b. Some other gaps also

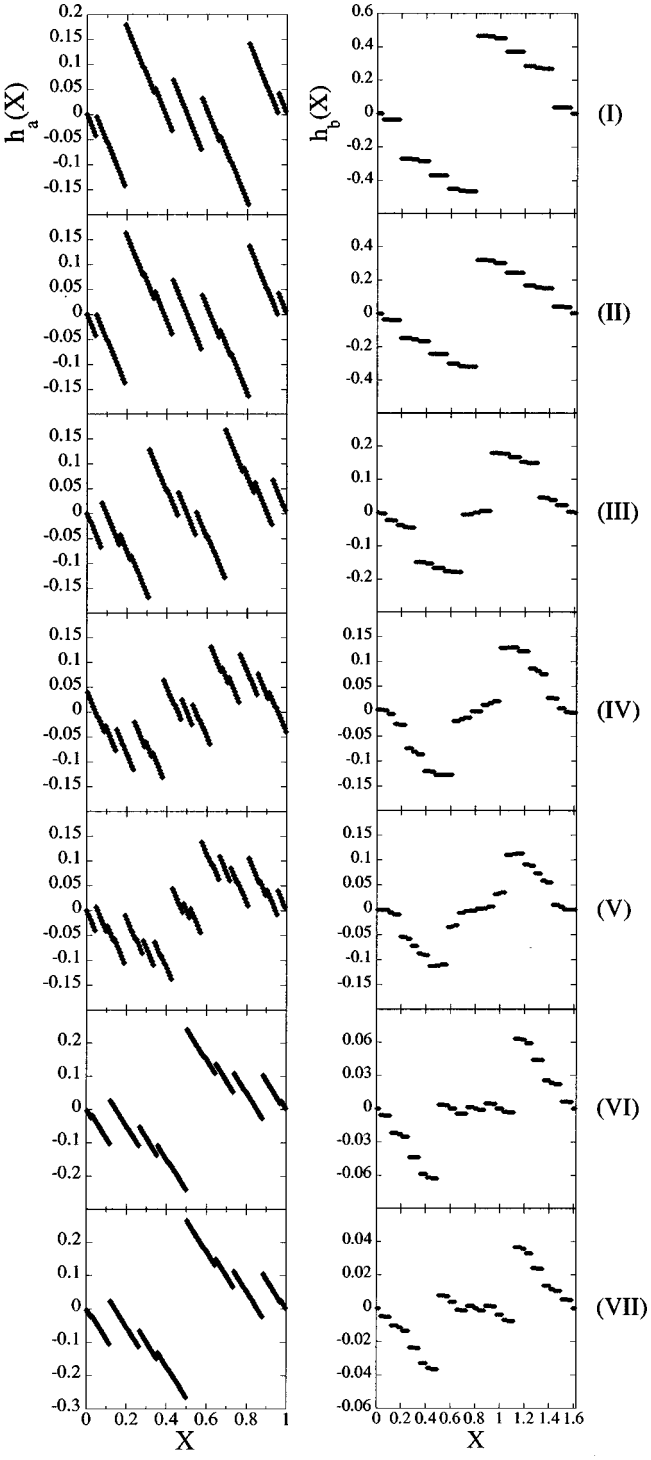

FIG. 4. Hull functions for $K_I=1$, $K_a=1$, and $K_s=1$. The graphs in the left (right) row are the hull functions for the upper (lower) chain. The values of K_b, (I) 0.1, (II) 0.702, (III) 1.3, (IV) 1.83, (V) 2.11, (VI) 4.09, and (VII) 8.14, correspond to arrows indicated in Fig. 2(a).

vanish or shrink, otherwise enlarge, and furthermore new gaps appear at several positions. Fig. 4(III)–4(V) show h_a and h_b at several values of K_b, where $\omega^2_{\rm lpf}$ shows a local maximum against the change in K_b [see arrows (III)–(V) in Fig. 2(a)]. It should be noted here that the gap structures of h_a and h_b shown in (III)–(V) in Fig. 4 are different from each other. In a K_b regime between two nearest-neighbor

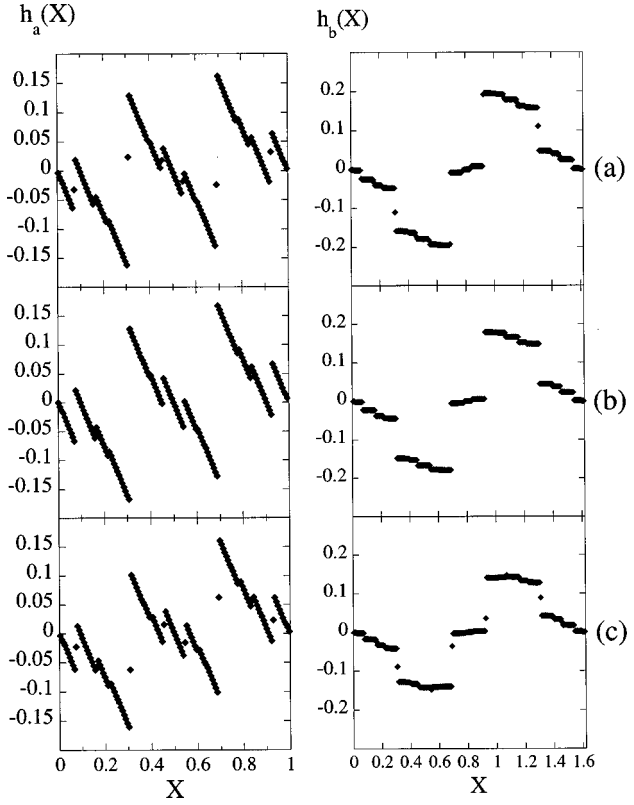

FIG. 5. Hull functions for $K_I=1$, $K_a=1$, and $K_s=1$. The values of K_b are (a) 1.18, (b) 1.3, and (c) 1.58, where (a) and (c) correspond to local minima of $\omega^2_{\rm lpf}$ and (b) corresponds to a local maximum of $\omega^2_{\rm lpf}$ indicated by the arrow (III) in Fig. 2(a).

valleys of $\omega^2_{\rm lpf}$, both the gap structures of h_a and h_b, are almost unchanged. Only when K_b is changed crossing through the valley of $\omega^2_{\rm lpf}$, the gap structures are suddenly changed, i.e., new gaps appear. In the large K_b regime ($K_b>2.4$), as shown in (VI) in Fig. 4, the central gap appears in h_a, but it is absent in h_b, and the gaps of h_b as a whole are highly reduced. This behavior indicates that the upper chain is in the conventional breaking of the analyticity state due to the Aubry transition. These gap structures of h_a and h_b retain up to infinite K_b while the amplitude of h_b as a whole shrinks as K_b is increased [(VI) and (VII) in Fig. 4]. The $\omega^2_{\rm lpf}$ also does not change in this large K_b regime. To see how the change of gap structures of hull functions takes place at the valleys of $\omega^2_{\rm lpf}$, in Figs. 5(a) and 5(c), we show hull functions for two nearest-neighbor valleys (local minima) of $\omega^2_{\rm lpf}$ at $K_b=1.18$ and 1.58. Note here that the K_b for (III) in Fig. 4 is located in the K_b regime between these two nearest-neighbor valleys of $\omega^2_{\rm lpf}$. For the comparison with these states at valleys, the graph of (III) in Fig. 4 is plotted again in Fig. 5(b). In Figs. 5(a) and 5(c) several gaps of the hull functions observed in Fig. 5(b) are destroyed by the appearance of certain states in gaps, i.e., the formation of new gap structures at the K_b's. As mentioned above, the gap structures of hull functions for Fig. 5(b) are stable and almost unchanged in the regime of $1.18<K_b<1.58$ where no valley of $\omega^2_{\rm lpf}$ exists. Similar behavior is observed around each valley of $\omega^2_{\rm lpf}$. When K_b reaches one of the critical value, the old gap structure becomes unstable and new states appear in gaps, which accompany the decrease of the phonon gap and

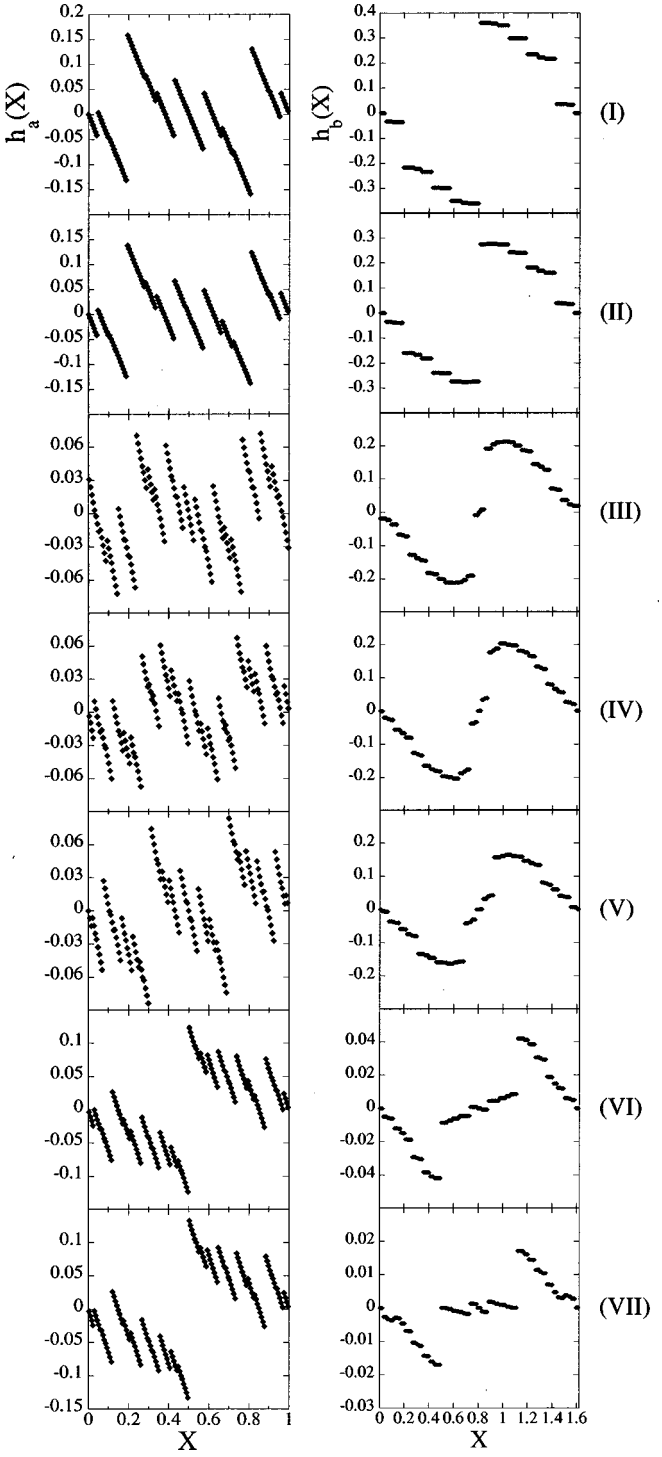

FIG. 6. Hull functions for $K_I=0.45$, $K_a=1$, and $K_s=1$. The values of K_b, (I) 0.01, (II) 0.15, (III) 0.27, (IV) 0.305, (V) 0.43, (VI) 3.21, and (VII) 9.71, correspond to arrows indicated in Fig. 2(b).

then the pinning force. When K_b crosses the critical value, new gap structure becomes stable and the phonon gap increases. Further change of K_b moves the system to the next critical value and then the successive phase transition occurs.

In Fig. 6 we show the hull functions h_a and h_b for several values of K_b in the case of weak interchain interaction $K_I=0.45$, and $K_s=1$, which are the same values with those in Fig. 2(b). In the small and large K_b regimes [(I), (II), and

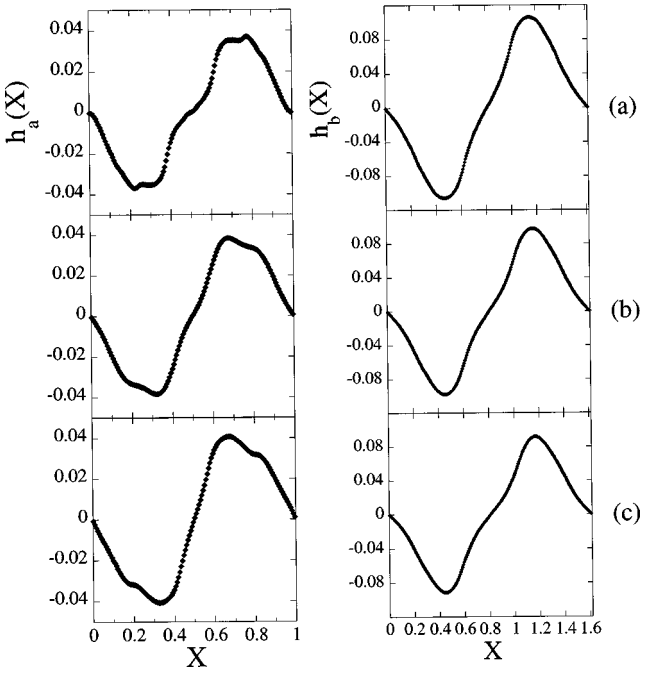

FIG. 7. Hull functions for $K_I=0.45$, $K_a=1$, and $K_s=1$. The values of K_b are (a) 0.8, (b) 0.9, and (c) 1.0.

(VI), (VII) in Figs. 6, respectively] where ω^2_{lpf} is almost constant, both the gap structures of h_a and h_b are unchanged, one of which shows the central gap. This indicates that one of the upper and lower chains is in the conventional breaking of the analyticity state due to the Aubry transition in the large and small K_b regime, respectively. In the intermediate regime [(III)–(V) in Fig. 6], the gap structures as a whole are rather sensitive to the change in K_b, but also in this case the gap structures are almost unchanged in a small K_b regime between two nearest-neighbor valleys of ω^2_{lpf}. Thus, the behavior of h_a and h_b is similar to that in Fig. 4 in this regime. However, in the K_b regime $0.6<K_b<1.4$, for $K_I=0.45$, where ω^2_{lpf} is vanishing, both the hull functions show a peculiar feature. In Fig. 7 we show several typical h_a and h_b in this K_b regime. It is clearly observed that both hull functions h_a and h_b are continuous and show sinusoidal forms, which are quite similar to that of the hull function for the FK model in the absence of the breaking of analyticity. These correspond to states in which all atoms of both chains locate near its regular sites periodically and are weakly affected by the almost sinusoidal interchain force caused by atoms in the other chain. Since the continuous hull functions mean that the atomic distribution is spatially continuous both in the upper and lower chains, every atom in the upper chain moves smoothly when the upper chain is driven by the external force. Therefore, there are no energy costs against the sliding motion of the upper chain. Hence the maximum static frictional force vanishes as observed in Fig. 2(b).

For $K_s=10$ and $K_I=1$ [(I)–(IV) in Fig. 8], h_a does not show any remarkable changes of gap structures. h_b gradually changes its gap structure only in a large K_b regime ($K_b>10$), but the effect of the change is almost negligible because the amplitude of the gaps of h_b becomes very small for such large K_b's. Therefore, all elastic effects come from the upper chain. The behavior of the hull functions reflects the

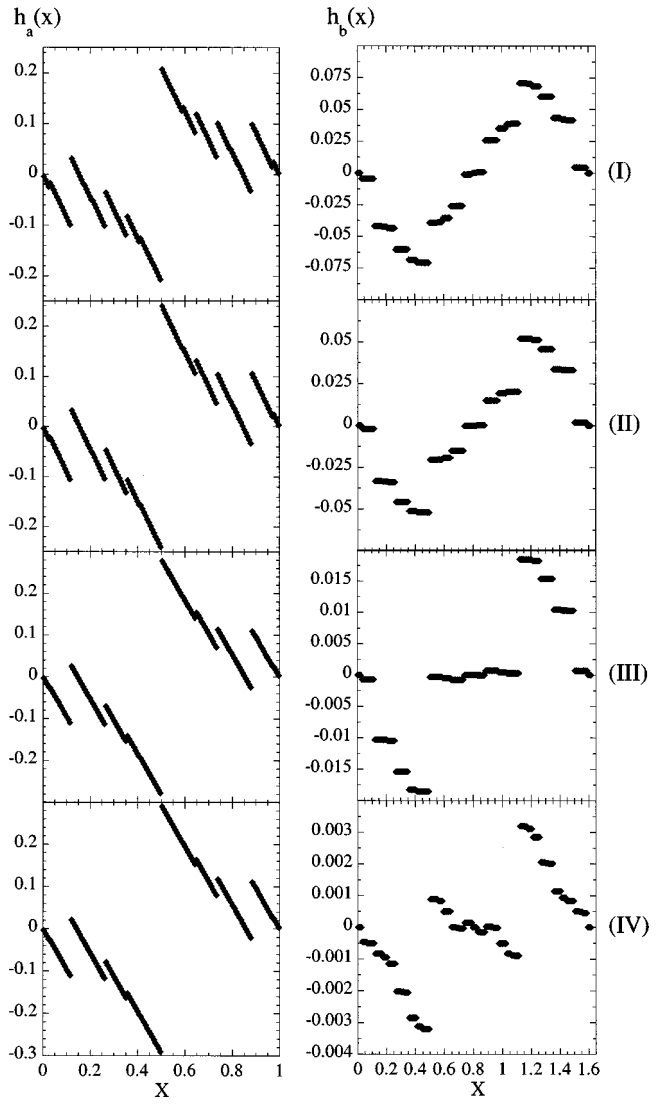

FIG. 8. Hull functions for $K_I=1$, $K_a=1$, and $K_s=10$. The graphs in the left (right) row are the hull functions for the upper (lower) chain. The values of K_b, (I) 0.01, (II) 1, (III) 10, and (IV) 100, correspond to arrows indicated in Fig. 2(c).

smooth change in the phonon gap in Fig. 1(c). In all regime of K_b, h_a shows the largest central gap, but h_b does not. Thus, in these pinned states the conventional breaking of analyticity due to the Aubry transition occurs in the upper chain for the whole range of K_b. Then the magnitude of the central gap in h_a is quite larger than those of the gaps in h_b and almost unchanged against the change in K_b.

It can be confirmed that the breaking of the analyticity states exist in the present two-chain model, but they are rather complicated and different from the conventional one due to the Aubry transition of the FK model. In the small (large) K_b regime, however, the gap structure of h_b (h_a) is the same as the conventional one observed in the breaking of the analyticity state in the FK model, while that of h_a (h_b) is different. That is, in the two-chain model, it is considered that whether the conventional breaking of the analyticity state characterized by the largest central gap exists in the upper or lower chain depends on the elasticity of the two chains. When the lower (upper) chain is highly stiffer than the upper (lower) one, i.e., K_b/K_a or $K_s/K_a \gg 1$ ($\ll 1$), the atoms in the upper (lower) chain tend to relax into potential minima created by the atoms in the lower (upper) chain, and then the conventional breaking of the analyticity state appears in the upper (lower) chain. In the intermediate K_b regime, however, quite different states from the conventional breaking of the analyticity state observed for the FK model appear. We will again discuss this point later by calculating the energy quantities of the system.

It should be noted here that all the hull functions shown in Figs. 4–8 do not contain irregular points that break a rotational symmetry by π of hull functions. This fact means that atomic configurations obtained above are not disordered, but they exactly reflect the discreteness of hull functions in an incommensurate system. This feature of the pinned atomic configuration is the same as that for the FK model.[10]

It is helpful here to observe the change of the pinned lattice structures in real space. Figure 9 shows the local lattice structure in the pinned state for $K_I=1$ and $K_s=1$, which are the same values with those in Figs. 2(a), 3(a) and 4. Here the atomic displacements from the regular periodic sites in the two chains δu_i and δv_i are plotted in Figs. 9(a) and 9(b), respectively, for K_b's indicated by arrows (II)–(VI) in Fig. 2(a). In the small K_b regime ($K_b<0.8$), the lattice structure is essentially unchanged [(1) in Figs. 9(a) and 9(b)]. In the intermediate regime ($0.8<K_b<2.4$), however, both δu_i and δv_i are very sensitive to the change in K_b. Figures (2) and (3) in Figs. 9(a) and 9(b) correspond to atomic displacements at local maxima of the phonon gap $\omega^2_{\rm lpf}$ in Fig. 2(a). It is obvious that the spatial modulation patterns of δu_i and δv_i show quasiperiodicity approximately for each K_b, but the spatial patterns are different for different values of K_b. When K_b increases further ($K_b>2.5$), the reconstruction does not occur any more and the lattice structures as observed in (5) in Figs. 9(a) and 9(b) retain up to infinite K_b, but the atomic displacement in the lower chain δv_i as a whole decreases its magnitude more and more. Similar changes of local lattice structures are observed also in the intermediate K_b regime for $K_I=0.45$ and $K_s=1$. Note here that if the behavior of the phonon gap has a self-similar nature as noticed in Fig. 2(a), then infinite sorts of local lattice structures would exist in the intermediate K_b regime.

4. Analysis of energy and discussion on the pinning mechanism

We discuss further the anomalous pinning behavior by examining the energy of the system. Here it is useful to define the following energy quantities. Elastic energy in the upper chain $E_{\text{ela-}a}$ and that in the lower chain $E_{\text{ela-}b}$ are given by

$$E_{\text{ela-}a}=\frac{K_a}{2}\sum_i^{N_a}(u_{i+1}-u_i-c_a)^2, \tag{12}$$

$$E_{\text{ela-}b}=\frac{K_b}{2}\sum_i^{N_b}(v_{i+1}-v_i-c_b)^2. \tag{13}$$

Elastic energy between the lower chain and the substrate $E_{\text{ela-}s}$ is given by

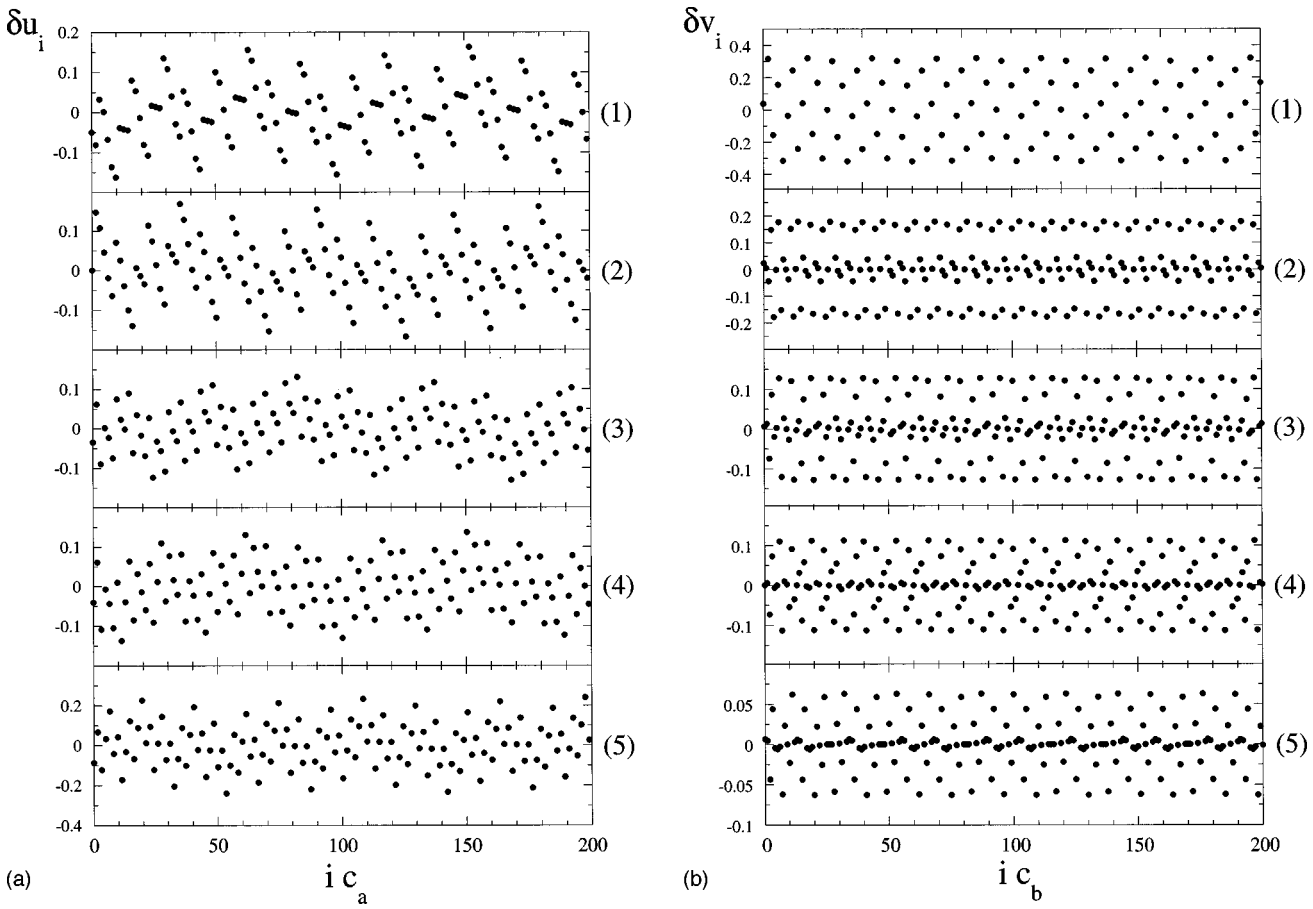

FIG. 9. Local lattice structures of the upper and lower chains for $K_I=1$, $K_a=1$, and $K_s=1$. Local atomic displacements δu_i and δv_j are plotted against periodic regular sites ic_a and jc_b in (a) and (b), respectively. The values of K_b are (1) 0.702, (2) 1.3, (3) 1.83, (4) 2.11, and (5) 4.09, which correspond to arrows (II), (III), (IV), (V), and (VI) in Fig. 2(a), respectively.

$$E_{\text{ela-}s}=\frac{K_s}{2}\sum_{i}^{N_b}(v_i-ic_b)^2. \tag{14}$$

Total elastic energy $E_{\text{ela-total}}$ is the sum of

$$E_{\text{ela-total}}=E_{\text{ela-}a}+E_{\text{ela-}b}+E_{\text{ela-}s}. \tag{15}$$

Interchain interaction energy E_{int} is expressed as

$$E_{\text{int}}=\frac{1}{2}\sum_{i}^{N_a}\sum_{j}^{N_b}[U_I(u_i-v_j)-U_I(ic_a-jc_b)], \tag{16}$$

where the contribution in the case of periodic rigid atomic configurations is subtracted. To evaluate Eqs. (12)–(16) we used the atomic configuration obtained in the calculation of ω_{lpf}^2. Figures 10(a)–10(d) show these energy quantities plotted against K_b for $K_I=1$ and $K_s=1$, which are the same values with those in Figs. 2(a), 3(a), 4, 5, and 9. When K_b is very small ($K_b\ll 1$), the absolute value of the interchain interaction energy $|E_{\text{int}}|$ is much greater than $E_{\text{ela-}a}$, but not so much greater than $E_{\text{ela-}s}$. The upper chain deforms little, but the lower chain deforms so large to gain the interchain interaction. In fact the hull function of the lower chain h_b shows the central largest gap, but h_a does not and its magnitude is small. These behaviors indicate that the upper chain has an almost periodic structure, but the lower chain adjusts its local period to that of the upper chain to gain the interchain interaction, that is, the lower chain forms a kind of discommensurate structure or the soliton lattice. When K_b is increased, the deformation of the lower chain and $E_{\text{ela-}s}$ decrease. On the other hand, $E_{\text{ela-}b}$ increases because its coupling constant, itself, increases. When $|E_{\text{int}}|$ becomes comparable to the total elastic energy, the lattice structures of both chains in the small K_b regime becomes unstable and another structure appears. The presence of kinks for all energy curves in Fig. 10 indicates that the structural change is a phase transition of the first order. The difference in the lattice structures between phases is observable directly in Figs. 9(a) and 9(b). The disappearance of the central gap of the hull function h_b in Fig. 4 is attributed to the structural phase transition. Both chains form complicated discommensurate structures where both chains deform to make the local commensurate structure in order to gain the interchain interaction. The occurrence of the structural phase transition leads to the sudden decrease (or vanishing) of the phonon gap at $K_b\approx 0.81$ as observed in Fig. 2(a). In the intermediate K_b regime ($0.81<K_b<2.4$), many, or an infinite number of lattice structures appear there, each of which corresponds to a different discommensurate structure. When K_b is increased small or infinitesimally, lattice structures change to another one by a structural phase transition. Such phase transitions occur successively in this regime against the change in K_b. As the lower chain becomes stiffer, the atomic displacement in the lower chain δv_i is suppressed, and then $E_{\text{ela-}b}$ and $E_{\text{ela-}s}$

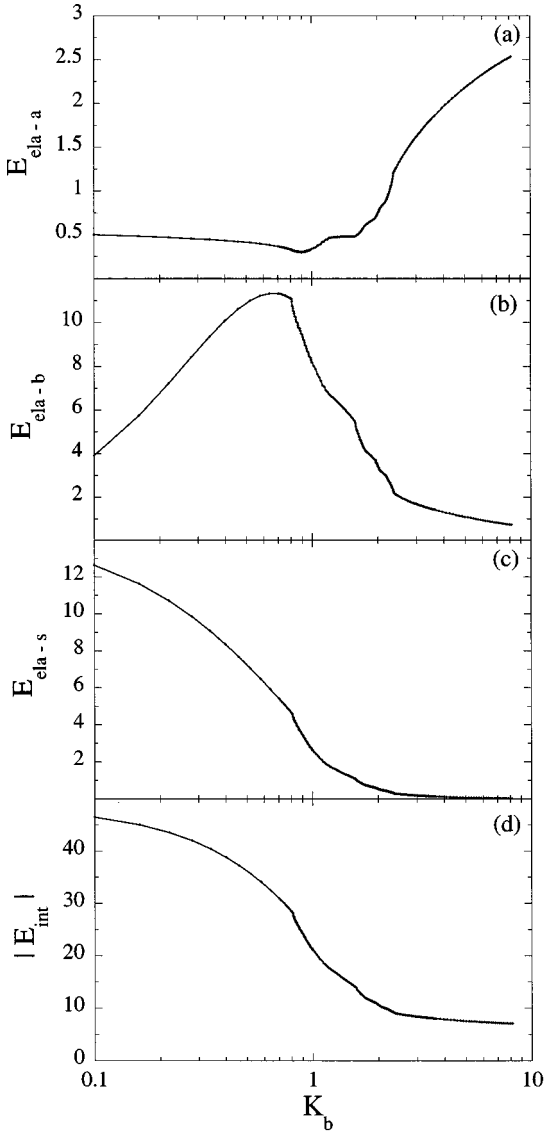

FIG. 10. Energy quantities vs K_b for $K_I=1$, $K_a=1$, and $K_s=1$; (a) $E_{\text{ela-}a}$, (b) $E_{\text{ela-}b}$, (c) $E_{\text{ela-}s}$, and (d) E_{int}.

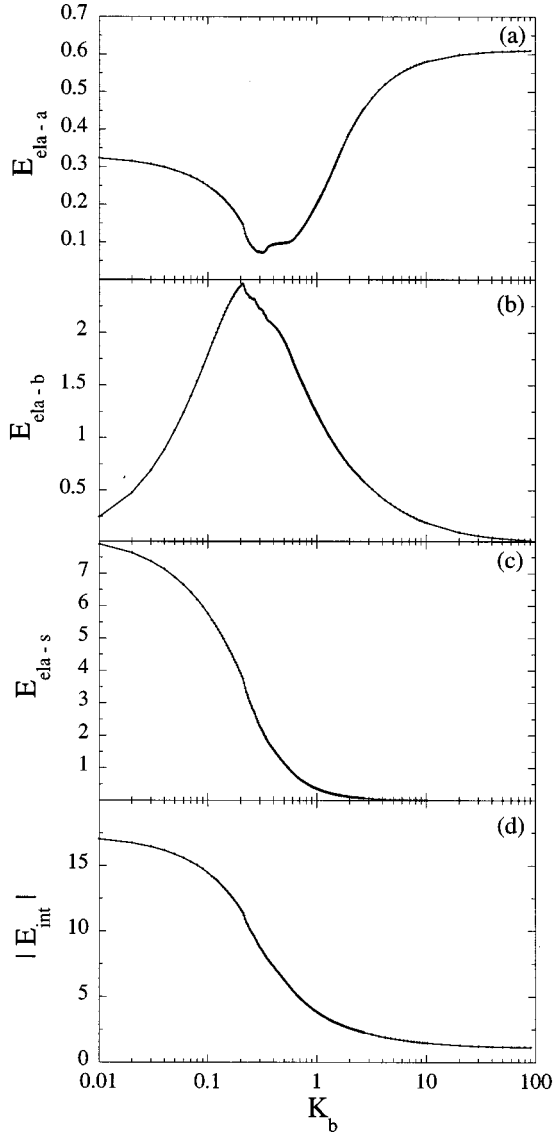

FIG. 11. Energy quantities vs K_b for $K_I=0.45$, $K_a=1$, and $K_s=1$; (a) $E_{\text{ela-}a}$, (b) $E_{\text{ela-}b}$, (c) $E_{\text{ela-}s}$, and (d) E_{int}.

decrease. Because in this K_b regime a slight change in K_b causes a structural phase transition, the phonon gap and the hull functions also change their structures correspondingly. It should be noted that the absence of the central gap in both hull functions characterizes the lattice structures in this intermediate K_b regime, where the successive structural phase transition occurs [Figs. 4(III)–4(V)]. This indicates complicated discommensurate structures of both chains. In the large K_b regime ($K_b>2.4$), the structural phase transition does not occur and a quite stable lattice structure appears in each chain, which is characterized by the largest central gap of h_a. These behaviors indicate that the lower chain forms an almost periodic structure, but the upper chain forms a discommensurate structure. In this regime the major contribution to $E_{\text{ela-total}}$ comes from $E_{\text{ela-}a}$ because the atomic displacement δv_i is suppressed and δu_i's are fixed into a locally commensurate configuration. Therefore, $E_{\text{ela-}a}$ and E_{int} are almost constant. Consequently, almost the same gap structures of the hull functions as those in Fig. 4(IV) and the same atomic configurations as those in (5) in Figs. 9(a) and 9(b) hold up to infinite K_b. We note here that these features, such as the kinks for energy and the vanishing of the phonon gap, which mean a first-order phase transition, are never expected in the case of the FK model because the Aubry transition observed in the FK model is a higher-order phase transition.

In Fig. 11 we show the energy quantities for the parameters $K_I=0.45$ and $K_s=1$ employed in Figs. 2(b), 3(b), 6, and 7. Also, in this case kinks are observed for all energy curves. Within the K_b regime ($0.6<K_b<1.4$) where the phonon gap and maximum-static frictional force are vanishing completely, any anomaly such as a kink is not observed. It is considered that one particular lattice structure of both chains appears in this K_b regime.

The energy quantities obtained for $K_s=10$ and $K_I=1$ are plotted in Figs. 12(a)–12(d). In this case, because of the large value of K_s, the lower chain is much stiffer than the upper chain. Then all energy quantities change smoothly with K_b. This means that these pinned states in all K_b regimes are understood essentially in the context of the conventional breaking of the analyticity state due to the Aubry transition for the FK model. Namely, the feature of pinned

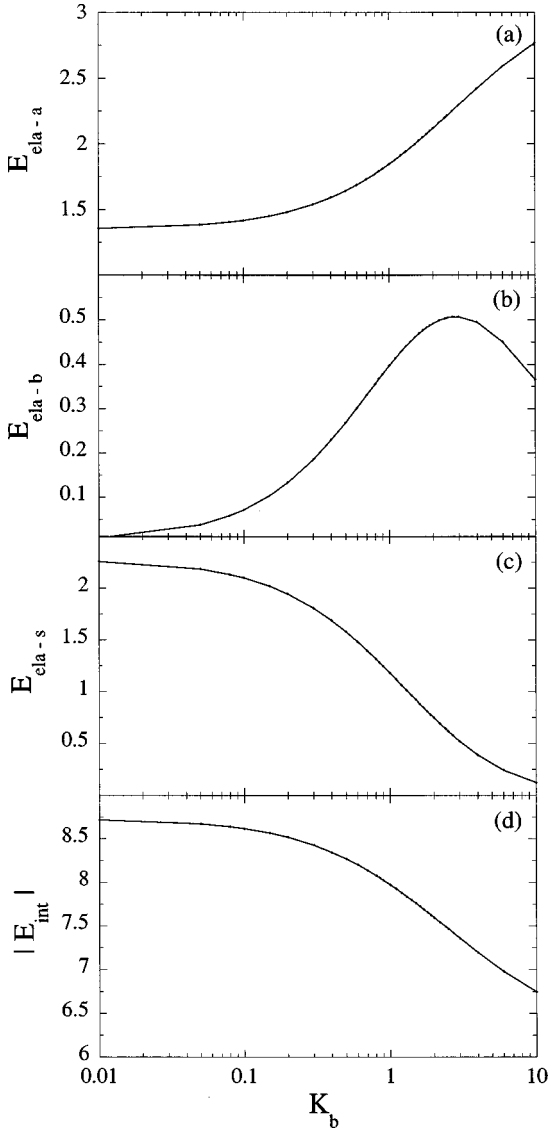

FIG. 12. Energy quantities vs K_b for $K_I=1$, $K_a=1$, and $K_s=10$; (a) $E_{\text{ela-}a}$, (b) $E_{\text{ela-}b}$, (c) $E_{\text{ela-}s}$, and (d) E_{int}.

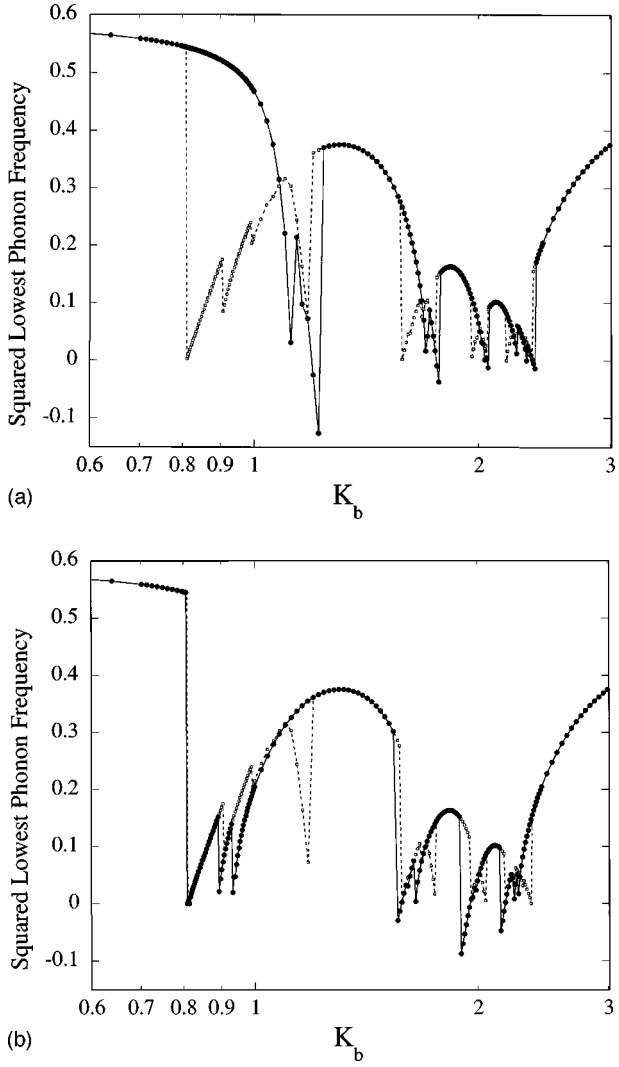

FIG. 13. Squared lowest-phonon frequency vs K_b for $K_I=K_s=1$. The solid lines with circles indicate the results obtained for the sweep with (a) increasing and (b) decreasing values of K_b. For comparison, the results in Fig. 2(a) are also plotted by the dashed lines with squares.

states for $K_s=10$ and $K_I=1$ are the same as those in the large K_b regime shown in Fig. 10, where $K_s=1$ and $K_I=1$.

For simplicity, we have changed the elasticity of the lower chain, while the elasticity of the upper chain is fixed (i.e., $K_a=1$). In general, it is considered that the relevant parameters to the pinning behavior of the present model are normalized ones: K_b/K_a, K_s/K_a, and K_I/K_a.

5. Hysteretic behavior of phonon gap

We have discussed the structural phase transitions of the first order. Then we expect hysteretic behaviors around the critical points. It is to be noted here that in all the results shown in Figs. 1–12, the initial configurations of atoms for each value of K_b are regular and periodic. In Fig. 13 we show phonon gaps for the same parameters ($K_I=K_s=1$) as those in Fig. 2(a) when K_b is swept, that is, the initial atomic configuration for a certain value of K_b is the final stable configuration for its previous value. The solid lines with circles indicate the results obtained for the sweep with (a) increasing and (b) decreasing value of K_b. For comparison, the results in Fig. 2(a) are also plotted by the dashed lines with squares. By comparison, between these two results, the hysteretic behavior of the phonon gap is obviously observed in the intermediate K_b regime. Such hysteretic behavior, which appears suddenly only in the intermediate K_b regime, is another evidence of the first-order phase transition.

We have considered only three initial conditions corresponding to a periodic atomic configuration (Figs. 2–12) and two history-dependent configurations (up and downward sweeps of K_b) (Fig. 13). The pinning behavior for other initial conditions has not been investigated exhaustively because a great variety of configurations may be considered. We have found here that the hysteresis curves of phonon gaps in Fig. 13 are reproducible well when the starting value of K_b for sweeps is set in the small or large K_b regime. Furthermore, even when the sweep of K_b is started from the intermediate regime, we have observed a tendency that phonon gaps change staying on one of the curves shown in Fig. 13 corresponding to the increase or decrease in the value of K_b.

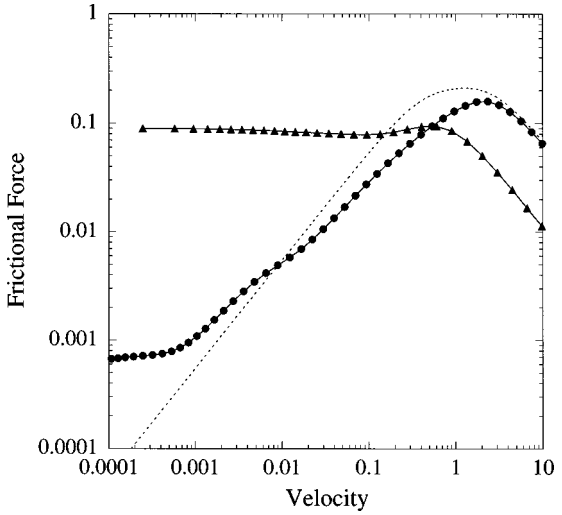

FIG. 14. Kinetic frictional force vs sliding velocity. Triangles denote numerical results obtained in the case that $K_b \to \infty$, $K_a = 1$, and $K_I = 1$, i.e., in a case of the FK model. Circles and dotted line denote a numerical result and an analytic result calculated with perturbation theory, respectively, for $K_I = 1$, $K_a = 1$, $K_b = 2$, and $K_s = 1$.

B. Sliding states

We here investigate the kinetic frictional force of the sliding state started from the pinned state. Figure 14 shows the kinetic frictional force as a function of the sliding velocity, where the interchain interaction is chosen as $K_I = 1$. The line with circles shows the result in the case that $K_b = 2$ and $K_s = 1$, which correspond to the valley of the maximum static frictional force in Fig. 3(a). For comparison, the result for a large K_b limit ($K_b = \infty$), where the present model corresponds to the FK model, is plotted in the same figure. The frictional force calculated by the perturbation theory[5,17] in the case that $K_b = 2$ and $K_s = 1$ is also plotted in this figure. It is found that the perturbation theory explains well the numerical results when the interchain interaction is so weak that the maximum static frictional force is vanishing.[17] For $K_b = 2$ and $K_s = 1$, the velocity-strengthening and velocity-weakening features of the kinetic frictional force are recovered and well explained by the perturbation theory. In the case of the FK model ($K_b = \infty$), however, the velocity-strengthening feature in the low-velocity regime is destroyed by the large maximum-static frictional force and the discrepancy between the simulation and the perturbation theory is obvious. Therefore, it is considered that the effect of the anomalous pinning in stationary states affects the sliding velocity dependence of the kinetic frictional force especially in a low-velocity regime.

Note here that no hysteretic behavior is observed in the velocity dependence of the kinetic frictional force between increasing and decreasing processes of the driving force when a periodic atomic configuration is employed as the initial state of no external force.

V. SUMMARY

We have investigated frictional phenomena of an incommensurate two-chain model. By controlling the elasticity of chains, we have found anomalous pinning behavior, which is accompanied by a successive phase transition. The pinned states show complicated behavior against the change in elastic parameters and differ apparently from the conventional breaking of the analyticity state due to the Aubry transition of the FK model. Under certain conditions on elasticity and interchain interaction, we have confirmed that the pinning force and the maximum-static frictional force are anomalously reduced or vanishing. Such anomalous pinning behavior is quite sensitive to the elasticity of chains, and it is never expected for the FK model because the anomalous pinning occurs in a characteristic regime where the elasticity of both chains becomes important.

We have also found that the anomalous pinning effect affects the kinetic frictional force significantly. Also, in such a pinned state the maximum-static frictional force is given in the vanishing velocity limit of the kinetic frictional force. In the case that the pinning force is weakened anomalously, the velocity dependence of the kinetic frictional force shows the velocity-strengthening and velocity-weakening features clearly, which are very close to those of the kinetic frictional force expected in the absence of the breaking of the analyticity state. In the present paper the overdamped sliding dynamics has been investigated in connection with the kinetic frictional force. For underdamped dynamics, however, the kinetic frictional force may show much more complicated velocity dependence, compared with the overdamped case.[19] It will be discussed in other reports.[19,20]

The detailed study of the overall phase diagram in the $K_b - K_I$ plane will be reported elsewhere. It might be interesting to investigate three-dimensional systems with relaxational interfaces. The breaking of analyticity is not restricted in one-dimensional systems and is also possible in higher dimensions, as noticed in Refs. 6 and 18. In practice, the relationship between the pinning effect and the elasticity of lattices in higher dimensions are an intriguing subject in tribology. We may expect more complicated pinning behavior than that for the present one-dimensional model.[21]

ACKNOWLEDGMENTS

This work was financially supported by Grants-in-Aid for Scientific Research of the Ministry of Education, Science, Sports and Culture. The computation in this work was done using the facilities of the Supercomputer Center, Institute for Solid State Physics, University of Tokyo.

[1] See, for example, articles in *Physics of Sliding Friction*, edited by B. N. J. Persson and E. Tosatti (Kluwer Academic, Dordrecht, 1996); *Sliding Friction*, edited by B. N. J. Persson (Springer, Berlin, 1998), and references therein.

[2] C. M. Mate, G. M. McClelland, R. Erlandsson, and S. Chiang, Phys. Rev. Lett. **59**, 1942 (1987).

[3] J. Krim and A. Widom, Phys. Rev. B **34**, 1403 (1986); A. Widom and J. Krim, *ibid.* **38**, 12 184 (1988); J. B. Sokoloff, J. Krim, and A. Widom, *ibid.* **48**, 9134 (1990).

[4] Y. Frenkel and T. Kontorova, Zh. Eksp. Teor. Fiz. **89**, 1340 (1938); **89**, 1349 (1938).

[5] J. B. Sokoloff, Phys. Rev. B **42**, 760 (1990); J. Appl. Phys. **72**, 1262 (1992); Phys. Rev. B **51**, 15 573 (1995).

[6] K. Shinjo and M. Hirano, Surf. Sci. **283**, 473 (1993).

[7] E. Granato, M. R. Baldan, and S. C. Ying, in *Physics of Sliding Friction* (Ref. 1).
[8] T. Strunz and F. J. Elmer, in *Physics of Sliding Friction* (Ref. 1); M. Weiss and F. J. Elmer, *ibid.*
[9] S. Aubry, in *Solitons and Condensed Matter Physics*, edited by A. R. Bishop and T. Schneider, Springer Series in Solid-State Sciences, Vol. 8 (Springer, Berlin, 1978).
[10] H. Peyrard and S. Aubry, J. Phys. C **16**, 1593 (1983).
[11] G. Theodorou and T. M. Rice, Phys. Rev. B **18**, 2840 (1978).
[12] S. Coutinho, P. Pitanga, and P. Lederer, Phys. Rev. B **23**, 4567 (1981).
[13] E. Allroth and H. Müller-Krumbhaar, Phys. Rev. A **27**, 1575 (1983).
[14] T. Ishii, J. Phys. Soc. Jpn. **52**, 168 (1983).
[15] H. Matsukawa and H. Fukuyama, Phys. Rev. B **49**, 17 286 (1994).
[16] H. Matsukawa and H. Fukuyama, *Physics of Sliding Friction* (Ref. 1).
[17] T. Kawaguchi and H. Matsukawa, Phys. Rev. B **56**, 13 932 (1997).
[18] M. Hirano and K. Shinjo, Phys. Rev. B **41**, 11 837 (1990).
[19] T. Kawaguchi and H. Matsukawa (unpublished).
[20] For the FK and FK-Tomlinson models, the underdamped sliding dynamics was investigated by Strunz, Weiss, and Elmer in Ref. 8.
[21] T. Kawaguchi and H. Matsukawa (unpublished).